Paper 66

IN-PLANE VORTEX-ROTOR INTERACTION AND ITS IMPACT ON ROTOR TRIM: AN ANALYTIC SOLUTION FOR ARBITRARY VORTEX ORIENTATION AND POSITION

Berend G. van der Wall, berend.vanderwall@dlr.de, DLR (Germany)

Lennert B. van der Wall, lvdw172@gmail.com

Abstract

The general aerodynamic problem of arbitrary oriented in-plane vortex-rotor interaction was investigated in the past only by numerical simulation. Just one special case of in-plane vortex-rotor interaction with the vortex axis in flight direction was recently solved analytically. In this paper the analytical solution for arbitrary in-plane vortex orientation and position relative to the rotor on thrust and hub moments is given that was published for the first time just before. Results provide the vortex impact on rotor trim (thrust, aerodynamic rolling and pitching moments about the hub) and the rotor controls required to mitigate these disturbances. In this paper the sensitivity of these results with respect to the main parameters will be given: the vortex core radius, its distance to the rotor center and its orientation angle relative to the rotor longitudinal axis, the rotor blade begin and end of the airfoiled section, and the advance ratio.

NOMENCLATUR

A, B	Non-dimensional effective begin and end of rotor blade, referenced to R
c	Airfoil chord, m
$C_{l\alpha}$	Lift curve slope, $C_{l\alpha} = 2\pi$
d_i	Radial integral coefficients, $d_i = (B^i - A^i)/i$; $i = 1,2,3,...$
L'	Blade element lift per unit span, N/m
M_x, M_y	Aerodynamic rotor rolling and pitching moment about the hub center
N_b	Number of rotor blades
r	Radial blade coordinate, m
r_a	Root cutout of the rotor blade, m
r_c	Vortex core radius, m
R	Rotor radius, m
T	Rotor thrust, N
v_{i0}	Induced velocity due to rotor thrust, m/s
v_{iV}	Vortex induced velocity, m/s
V_T, V_P	Velocities acting at the blade element tangential and perpendicular to the rotor disk, m/s
V_∞	Helicopter flight speed, m/s

x, y, z	Rotor coordinate system, x pos. downstream, y pos. starboard, z pos. up
x_0, y_0	Vortex closest point relative to the hub center, m
x_V, y_V, z_V	Vortex coordinate system
y_{V0}	Vortex distance relative to the rotor center, m
α	Blade element angle of attack, rad
α_S	Rotor shaft angle of attack, rad
Γ_V	Vortex circulation strength, m²/s
Δ	Perturbation of a variable
η	Geometric constant, $\eta = 2y_{V0}r_c$
Θ, Θ_0	Rotor blade pitch angle, collective control angle, rad
Θ_C, Θ_S	Rotor blade lateral and longitudinal cyclic control angles, rad
Θ_t	Linear rotor blade pre-twist angle, rad/R
λ_{i0}	Thrust-induced inflow ratio normal to the rotor disk, $\lambda_{i0} = v_{i0}/(\Omega R)$
λ_{iV}	Vortex-induced inflow ratio normal to the rotor disk, $\lambda_{iV} = v_{iV}/(\Omega R)$
λ_{V0}	Non-dimensional vortex strength, $\lambda_{V0} = \Gamma_V/(2\pi\Omega R^2)$
μ	Rotor advance ratio, $\mu = V_\infty \cos\alpha_S/(\Omega R)$
μ_z	Rotor axial inflow ratio, $\mu_z = -V_\infty \sin\alpha_S/(\Omega R)$
ξ	Transform of radial variable, $\xi = r^2 - y_{V0}^2 + r_c^2$
ρ	Air density, kg/m³
σ	Rotor solidity, $\sigma = N_b cR/(\pi R^2)$
ϕ	Inflow angle, rad, $\phi = \arctan V_P/V_T$
ψ	Rotor blade azimuth, rad, $\psi = \Omega t$
ψ_V	Vortex orientation angle relative to the rotor x-axis, rad
Ψ	Transform of rotor blade azimuth, $\Psi = \psi - \psi_V - \pi/2$
Ω	Rotor rotational speed, rad/s

1. INTRODUCTION

Vortex-rotor aerodynamic interaction is a phenomenon that was more intensely investigated by flight testing and by numerical simulation from the mid-1970s to the end of the 1980s with respect to flight mechanics response of helicopters encountering the wake of large and heavy fixed-wing aircraft [1]-[5]. The subject was taken up again from 2000 on for handling qualities aspects [6]-[8]. All these were based on numerical simulation with different degrees of simplifications. Computational fluid dynamics were also applied to the fundamental problem addressing the mutual vortex-wake interaction [9]. Recently a GARTEUR helicopter action group (HC-AG23) was investigating aspects of wind turbine blade tip vortices and their impact on helicopter operations in offshore wind farms [10].

The first entirely analytical solution based on blade element theory and steady aerodynamics was given 2017 for the special case of a vortex parallel to the x-axis of the rotor [11], [12]. Despite this being a case of the highest practical relevance – for example when helicopters perform air-refueling with a steady flight behind a tanker aircraft such as sketched in Fig. 1 – the general solution of in-plane vortex-rotor interaction with arbitrary position and orientation (including parallelism to the y-axis of the rotor) was still missing and left to numerical simulation. The analytical solution of this general problem is given in [13] for the first time.
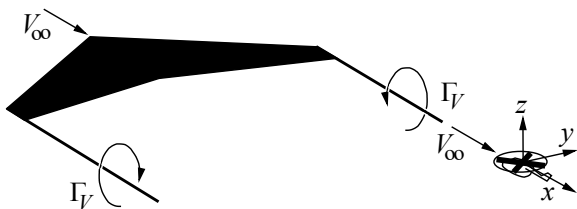

Fig. 1. Helicopter in the wake of a fixed-wing aircraft.

Oblique in-plane vortex-rotor interaction occurs when crossing a fixed-wing aircraft wake from the side or when flying in the wake of large wind turbines towards the turbine or away from it in wind direction. Although this kind of interaction will never be stationary and rather a transient process, the solution of the stationary interaction problem provides insight into the physics. This was solved only numerically in the past [14]-[16].

A clear differentiation must be made between the "classical" blade-vortex interaction (BVI), where a blade tip vortex generated by any of the rotor blades interacts with any rotor blade at any angle of interaction essentially in-plane of the rotor disk. These vortices have a core radius in the order of 15 % of the blade chord, which typically is about 7 % rotor radi-

us, thus the vortex core radius is in the order of 1 % of the rotor radius. In this article we focus on blade tip vortices generated by e.g. large fixed-wing aircraft, whose wing tip chord is about 10 times larger than that of the helicopter rotor blade, such that the wing vortex core radius is in the order of 10 % of the rotor radius, as used in the results section. While the classical BVI phenomenon requires fully unsteady aerodynamics treatment, the large wave length of the fixed-wing vortex interaction with the rotor blades may still be treated by quasi-steady blade element momentum theory.

Because the derivation of the analytical solution is already provided in [13] this will not be repeated here, just the final results are given. This paper focuses on the results that can be obtained by this solution, their sensitivity to the relevant non-dimensional parameters, as are: the vortex core radius r_c (referenced to the rotor radius), its distance to the rotor hub center y_{V0} and its orientation angle relative to the rotor longitudinal axis ψ_V, the effective aerodynamic begin $r_a = AR$ and end BR of the rotor blade airfoiled sections, and the advance ratio of the rotor μ.

2. TECHNICAL APPROACH

2.1. Problem definition

The vortex-rotor interaction problem is treated here by an infinite long space-fixed straight-line vortex lying in the plane of the rotor disk at any distance (x_0, y_0) to the rotor center and any angle of orientation ψ_V with respect to the rotor x-axis, see Fig. 2 (a). Any mutual interactions of the vortex and the rotor wake are ignored.

The rotor has N_b blades of constant chord c and an airfoiled part of it extending from the inner root cutout $r_a \geq 0$ to its radius R in steady forward flight with speed $V_\infty \geq 0$. Helicopter trim in forward flight requires the rotor slightly tilted forward by the shaft angle of attack $\alpha_S < 0$, depending on flight speed. Blade element theory computes the blade section lift based on the flow components in-plane and normal to the radial axis of the blade, V_T, and perpendicular to the rotor disk, V_P, and the blade pitch angle, see Fig. 2 (b). The rotor blade rotates in counter-clockwise direction as seen from above at a rotational speed of Ω and its azimuth angle is ψ.

The tangential velocity consists of the rotational speed at the respective radial station Ωr and the periodic contribution of the speed of flight $V_\infty \cos \alpha_S \sin \psi$, while the perpendicular component (positive downwards) includes a constant contribution caused by flight speed and rotor inclination $-V_\infty \sin \alpha_S$, the induced velocity v_{i0} caused by the
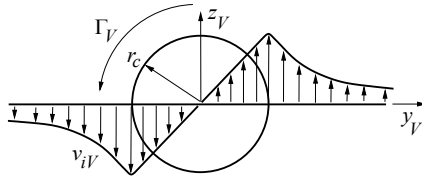
rotor thrust (also assumed as constant), and the induced velocity caused by the vortex v_{iV}, which is a nonlinear function of both rotor radial coordinate and azimuth position.
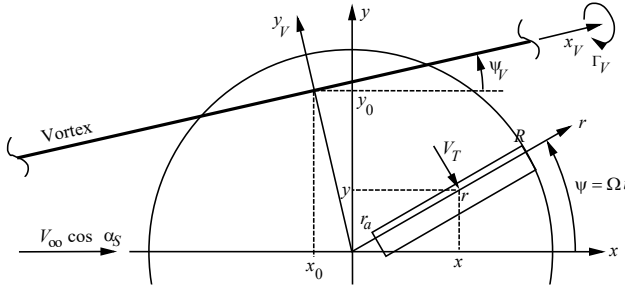
(a) Top view on rotor disk
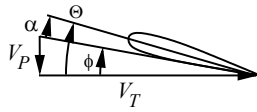
(b) Velocities and angles at the blade element

(c) Vortex-induced velocity profile

Fig. 2. Rotor disk with in-plane vortex.

The vortex-induced velocity field sketched in Fig. 2 (c) can be represented by its circulation strength Γ_V (the sign denotes its sense of rotation), its core radius r_c and the location normal to the vortex axis y_V in the following manner, where x, y are the coordinates of the blade element of interest, see Fig. 2 (a). This is a special case of the "Vatistas" vortex swirl velocity model [17] frequently used in the literature.

$$V_T\left(r,\psi\right)=\Omega r+V_\infty \cos\alpha_S \sin\psi$$

$$(1) \quad V_P\left(r,\psi\right)=-V_\infty \sin\alpha_S +v_{i0}+v_{iV}\left(r,\psi\right)$$

$$v_{iV}\left(r,\psi\right)=-\frac{\Gamma_V}{2\pi}\frac{y_V\left(r,\psi\right)}{y_V^2\left(r,\psi\right)+r_c^2}$$

As shown in Fig. 2 (b), these components generate an inflow angle ϕ that has to be considered for computation of the aerodynamic angle of attack $\alpha = \Theta - \phi$ at the blade element having a local pitch angle Θ relative to the rotor disk, which consists of a linear built-in pre-twist relative to 75 % radius $\Theta_t(r-0.75R)$ and the pilot collective, lateral and longitudinal cyclic control angles $\Theta_0, \Theta_C, \Theta_S$.

Applying small angle assumption and with the inflow angle thus simplified to $\phi = \arctan(V_P/V_T) \approx V_P/V_T$ from Fig. 2 (b) the section angle of attack becomes

$$\alpha\left(r,\psi\right)=\Theta\left(r,\psi\right)-\phi\left(r,\psi\right)$$
$$(2) \quad \approx \Theta_0 +\Theta_C \cos\psi +\Theta_S \sin\psi +$$
$$\Theta_t\left(r-0.75R\right)-V_P\left(r,\psi\right)/V_T\left(r,\psi\right)$$

An important parameter is the vortex distance from the rotor hub center y_{V0} in a coordinate system parallel to the vortex coordinates, i.e. rotated by ψ_V.

$$(3) \quad y_{V0}=y_0 \cos\psi_V -x_0 \sin\psi_V$$

Linear blade element momentum theory provides the section lift per unit span, L'. It is computed in blade element theory by the dynamic pressure based on air density ρ and the tangential velocity V_T, the chord length c, the lift curve slope $C_{l\alpha}$ (which is assumed constant), and the angle of attack α. Stall, compressibility and other nonlinearities are neglected here. Based on the local lift the steady values of rotor thrust T and of the aerodynamic rolling and pitching moments M_x, M_y can be computed by dual integration over the azimuth and the radial coordinate, and consideration of the number of blades N_b.

$$(4) \quad L'\left(r,\psi\right)=\frac{\rho}{2}V_T^2\left(r,\psi\right)cC_{l\alpha}\alpha\left(r,\psi\right)$$

The next step is to introduce dimensionless expressions. All coordinates, lengths and the core radius are divided by the rotor radius R, all velocities by the rotor tip speed ΩR, lift per unit span by $\rho(\Omega R)^2\pi R$, thrust by $\rho(\Omega R)^2\pi R^2$ and the aerodynamic hub moments by $\rho(\Omega R)^2\pi R^2 R$. Regarding the velocities this generates the advance ratio μ, the axial inflow ratio μ_z, the induced inflow ratio caused by the rotor thrust λ_{i0}, the vortex-induced inflow ratio λ_{iV}, and the non-dimensional vortex strength λ_{V0}. The vortex-induced velocities are provided in the vortex axis system, which requires a coordinate transform from the rotor azimuth into an azimuth relative to the vortex y_V-direction $\Psi = \psi - \psi_V - \pi/2$, which is zero when the rotor blade radial direction is oriented normal to the vortex axis. From Eq. (1) the vortex-induced inflow ratio becomes

$$\lambda_{iV}=-\lambda_{V0}\frac{y_V\left(r,\Psi\right)}{y_V^2\left(r,\Psi\right)+r_c^2}$$

$$(5)$$

$$\lambda_{V0}=\frac{\Gamma_V}{2\pi\Omega R^2}$$

with the blade element position in the vortex coordinate system of

$$
y_V(r,\psi) = (r\sin\psi - y_0)\cos\psi_V
$$
(6)
$$
- (r\cos\psi - x_0)\sin\psi_V
$$
$$
= r\cos\Psi - y_{V0} = y_V(r,\Psi)
$$

2.2. Analytical solution

Due to the linear superposition of the vortex-induced velocities and thus the vortex-induced lift the rotor trim in undisturbed air is completely separated from the vortex impact. Thus, the additional control angles $\Delta\Theta_0, \Delta\Theta_C, \Delta\Theta_S$ required to mitigate the vortex impact on trim can be calculated separately. The full details are given in [13].

Because the vortex strength λ_{V0} is a linear multiplier in vortex-induced thrust and its aerodynamic hub moments the ratio $\Delta\Theta/\lambda_{V0}$ is a measure for the magnitude of vortex-rotor interaction. It turns out – as in the case of trim in undisturbed air – that the collective and longitudinal cyclic control angles are coupled in forward flight and the lateral cyclic control angle remains separated from these. The computation of rotor controls required to mitigate the vortex-induced impact on trim results in the following expressions, for details see [13]. In the following $\overline{\Delta T} = \Delta T/(\lambda_{V0}\sigma C_{l\alpha})$ and analogous for the moments.

$$
\frac{1}{\lambda_{V0}}\left\{\begin{matrix}\Delta\Theta_0\\\Delta\Theta_S\end{matrix}\right\} = -\frac{\begin{bmatrix}a_{22} & -a_{12}\\-a_{21} & a_{11}\end{bmatrix}}{a_{11}a_{22}-a_{21}a_{12}}\left\{\begin{matrix}\overline{\Delta T}\\\overline{\Delta M_x}\end{matrix}\right\}
$$
(7)
$$
\frac{\Delta\Theta_C}{\lambda_{V0}} = -\frac{\overline{\Delta M_y}}{a_{33}}
$$

Therein, the system matrix elements $a_{ij}; i,j = 1,2,3$ are (i,j combinations not listed are zero)

$$
a_{11} = d_3 + \frac{\mu^2}{2}d_1 \qquad a_{12} = \mu d_2
$$
(8)
$$
a_{22} = \frac{d_4}{2} + \frac{3\mu^2}{8}d_2 \qquad a_{21} = \mu d_3
$$
$$
a_{33} = -\frac{d_4}{2} - \frac{\mu^2}{8}d_2 \qquad d_i = \frac{B^i - A^i}{i}
$$

In hover $\mu = 0$ and then $a_{12} = a_{21} = 0$, which decouples the collective and longitudinal cyclic control angles. With $C_V = \cos\psi_V$; $S_V = \sin\psi_V$ and the following abbreviations, see [13],

$$
G(\sqrt{+}) = \ln\left|1 + \frac{r_c}{\sqrt{+}}\right| + \frac{\ln\left|\sqrt{+}^2 + y_{V0}^2\right|}{2}
$$
(9)
$$
\sqrt{\pm} = \sqrt{\frac{1}{2}\left(\sqrt{\xi^2 + \eta^2} \pm \xi\right)}
$$
$$
\xi = r^2 - y_{V0}^2 + r_c^2
$$
$$
\eta = 2y_{V0}r_c
$$

the non-dimensional vortex-induced rotor thrust and its aerodynamic hub rolling and pitching moments are expressed by, see [13],

$$
\overline{\Delta T} = \left[\mu C_V G(\sqrt{+}) + \mathrm{sgn}(y_{V0})\sqrt{-}\right]_A^B
$$

$$
\left\{\begin{matrix}\overline{\Delta M_x}\\\overline{\Delta M_y}\end{matrix}\right\} = \begin{bmatrix}C_V & -S_V\\S_V & C_V\end{bmatrix}\left\{\begin{matrix}d_2\\0\end{matrix}\right\} +
$$

$$
+\mu\left(y_{V0}G(\sqrt{+}) + r_c\arctan\frac{y_{V0}}{\sqrt{+}}\right)_A^B\left\{\begin{matrix}C_V\\S_V\end{matrix}\right\}
$$

$$
+\begin{bmatrix}|y_{V0}| & -r_c\\-\mu S_V\mathrm{sgn}(y_{V0}) & 0\end{bmatrix}\left\{\begin{matrix}\sqrt{-}\big|_A^B\\\sqrt{+}\big|_A^B\end{matrix}\right\}
$$

(10)

It is interesting to note that neither the blade chord or rotor solidity (including the number of rotor blades) nor the lift curve slope enter the solution. This is because these parameters enter both the vortex-induced lift generation and the lift generation caused by the blade pitch angle in the same manner. Thus they eliminate from the solution, which from a physical point of view is only a matter of vortex-induced angles of attack and corresponding blade pitch angles.

2.3. Simplifications and limits of application

Several simplifications are made in order to be able to obtain the analytical solution of Eqs. (7) to (10). These are listed in the following:

- Linear quasi-steady two-dimensional aerodynamics, incompressible attached flow, no stall

- Rigid space-fixed infinite straight-line vortex

- Small perturbations, small angles assumption: $\sin\alpha \approx \alpha$; $\cos\alpha \approx 1$; $\tan^{-1}\alpha \approx \alpha$

- Ignorance of the reversed flow regime

- Dynamic pressure based on tangential velocity only

The small angle assumption applied to the $\tan^{-1}\alpha$ as applied in Eq. (2) is valid until $\alpha \approx 30$ deg. Especially the inboard regions with small tangential velocities are susceptible to violation of these. Helicopters usually have a blade tip speed around $\Omega R = 220$ m/s and a blade root cutout (= begin of airfoiled sections) of $A = 0.2$, i.e. 20% of the rotor radius, thus 44 m/s. Assume a vortex with a maximum vortex-induced velocity at its core radius of $v_{iV} = 10$ m/s, then the resulting vortex-induced angle of attack at the root cutout becomes almost 13 deg, well within the valid range of linearization. The limit of validity is reached at a radius of $A \approx 0.08$, well below typical root cutout values. For simplicity in analysis, the aerodynamic integration often is beginning at the rotor hub $A = 0$ where $V_T = 0$ m/s, thus the linearization leads to an infinite angle, while the arctan results in 90 deg.

A similar situation is experienced in forward flight, where a circle with diameter $r = \mu$ extends from the hub into the retreating side, at which circumference $V_T = 0$ m/s and within a band of $\Delta r \approx \pm 0.08$ around it violates the small angle assumption. Todays modern helicopters reach maximum advance ratios of $\mu = 0.4$, therefore at an azimuth of 270 deg the inner portion of the blade $A \leq r < \mu$ experiences reversed flow with up to $V_T = \Omega R(A - \mu) = -33$ m/s at the root cutout. However, the lift is computed by multiplication of the angle of attack in Eq. (2) by the dynamic pressure, i.e. V_T^2, which results into $V_T V_P$. Therefore, within the usual range of blade root cutouts and up to the usual advance ratios the integral error made by the linearization and reversed flow is small on the rotor thrust, and even less on the aerodynamic hub moments because these additionally include the radial coordinate as multiplier.

3. RESULTS

In the results shown, one of the essential parameters – the distance of the vortex axis relative to the hub center in the vortex coordinate system – is varied from two rotor radii of the one side to the same distance on the other, $-2 \leq y_{V0} \leq +2$. Another important parameter is the vortex orientation with respect to the rotor x-axis, which varies in the range $-\pi \leq \psi_V \leq +\pi$, as illustrated in Fig. 3 (b).

In that figure, when $y_{V0} = \pm 1$, the vortex is the tangent to the rotor disk and when $y_{V0} = 0$ it is crossing the rotor center, while its orientation ψ_V remains constant. When $\psi_V = 0$ the vortex is always parallel to the rotor x-axis and $y_{V0} = y$, and for $\psi_V = \pm\pi$ it remains parallel to the rotor x-axis, but the sense of rotation as seen by the rotor blades becomes oppo-

site and $y_{V0} = -y$. In the case of $\psi_V = \pi/2$ the vortex is always parallel to the y-axis of the rotor and $y_{V0} = -x$, and in analogy to the former for $\psi_V = -\pi/2$ it remains parallel to the rotor y-axis, but the sense of rotation as seen by the rotor blades becomes opposite and $y_{V0} = x$.

3.1. Hover

Although from a physical point of view a stationary interaction of an external vortex with a rotor cannot exist this case is investigated first because of the fundamental physical insight that is provided by this case. Due to rotational symmetry of the dynamic pressure at the rotor blades the rotor controls to mitigate the vortex influence on rotor trim are completely decoupled, see Eqs. (7) and (8).

(a) Top view on rotor disk

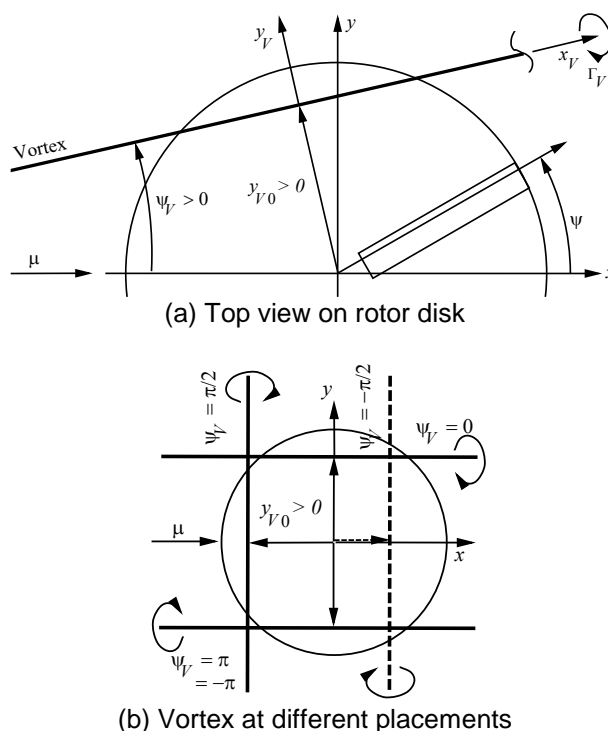(b) Vortex at different placements

Fig. 3. Variation of vortex position and orientation.

The representative parameters of the rotor are an effective begin of the airfoiled section at $A = 0.25$ and an effective end (representing tip losses) at $B = 0.97$. A vortex with a positive sense of rotation ($\lambda_{V0} > 0$) with a core radius of $r_c = 0.1$, i.e. 10% of the rotor radius, is used. These parameters are kept constant throughout the entire section 3.1 from Fig. 4 to Fig. 6 and a variation of all these parameters will follow in section 3.2. In hover (sections 3.1 and 3.2), the advance ratio is zero: $\mu = 0$.
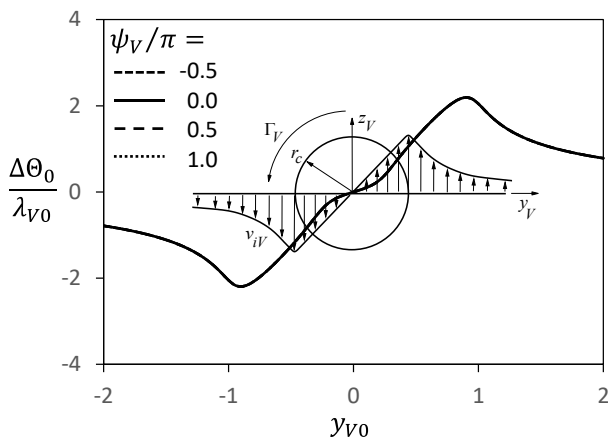
The collective control angle for vortex disturbance rejection on rotor thrust, related to the vortex strength $\Delta\Theta_0/\lambda_{V0}$, is shown in Fig. 4 (a) for the entire

range of the aforementioned vortex distance to the rotor center y_{V0} of ± 2 rotor radii and the range of vortex orientation once around the rotor $-\pi \le \psi_V \le \pi$, see Fig. 3 for better understanding. As can be seen from Fig. 4 (a), the collective control angle in hover does only depend on y_{V0} and is fully independent on ψ_V.

Four special cases of vortex orientation are sketched in Fig. 3 (b): $\psi_V = 0$ and $\pm \pi$ are parallel to the x-axis, while $\psi_V = \pm 0.5\pi$ are parallel to the rotor y-axis. Four cuts at these vortex orientation angles are shown in Fig. 4 (b) together with a vortex and its swirl velocity field placed in the rotor center, i.e. for $y_{V0} = 0$. Its sense of rotation agrees with Fig. 3.
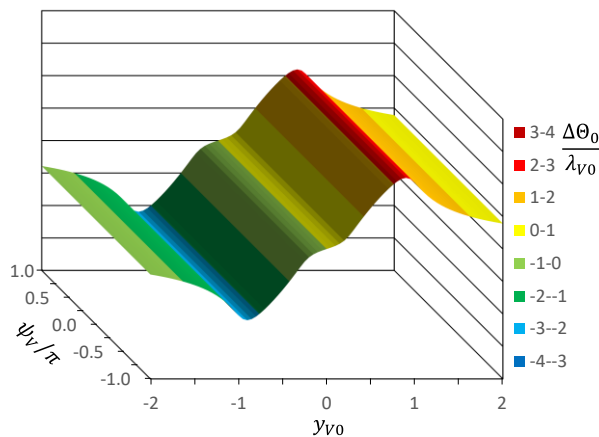
(a) Range of vortex position and orientation angles

(b) Selected vortex orientation angles

Fig. 4. Collective control angle for vortex disturbance rejection on rotor thrust.

From this vortex position it is immediately obvious that to the right of it there is as much upwash as it is downwash to the left of it, thus the impact on thrust must be zero and consequently the collective control angle must be zero as well. Shifting the vortex to the right to $y_{V0} = 1$, then the entire rotor disk is immersed in its downwash and the associated loss of

thrust must be compensated by a positive collective control angle, as is the case in the graph.

Contrary, shifting the vortex to the opposite end of the disk to $y_{V0} = -1$ the entire disk is immersed in its upwash and the associated gain in thrust must be compensated by a negative collective control angle, as shown by the graph. Further outside positions diminish the vortex-induced velocities, thus the impact on thrust, and as well the amount of collective control angle required to mitigate this and the curves asymptotically approach zero for very large distances of the vortex as required.
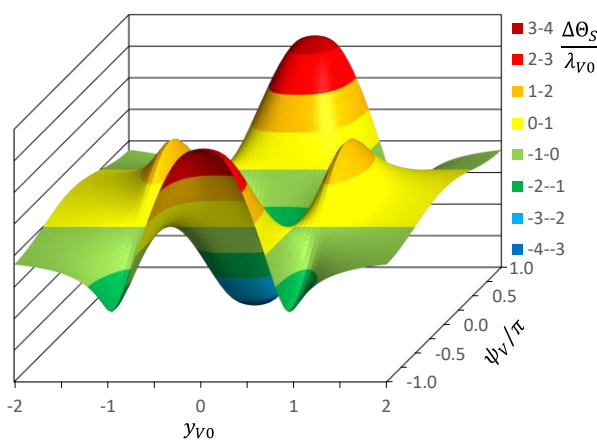
The longitudinal cyclic control angle required for vortex disturbance rejection on the aerodynamic rotor rolling moment, related to the vortex strength $\Delta\Theta_S/\lambda_{V0}$, is shown in Fig. 5 (a) for the same range of y_{V0} and ψ_V as before.

Contrary to the collective control angle, the longitudinal cyclic control angle in hover significantly depends on both the vortex distance to the rotor center and its orientation relative to the rotor x-axis. The dependency on the vortex orientation angle is logical because only lateral asymmetries of vortex-induced velocities generate aerodynamic rolling moments. Therefore, vortex orientation parallel to the rotor y-axis, i.e. $\psi_V = \pm 0.5\pi$, generate lateral symmetry of vortex-induced velocities, therefore no aerodynamic rolling moment and thus zero longitudinal cyclic control is needed.
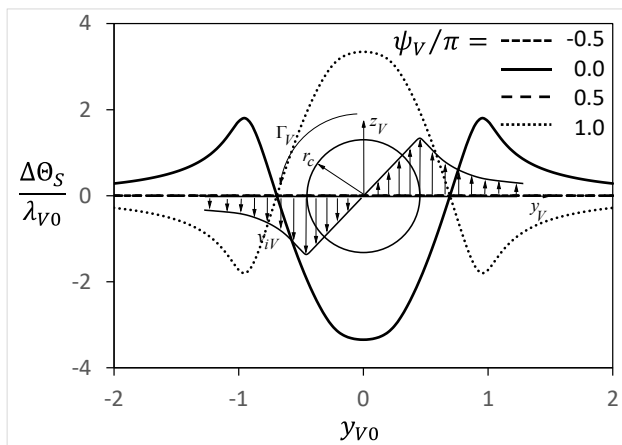
Four cuts at vortex orientation angles $\psi_V = 0, \pm 0.5\pi, \pi$ are shown in Fig. 5 (b) together with a vortex and its swirl velocity field placed in the rotor center. For $\psi_V = 0$ this generates a large upwash on the advancing side of the rotor and as much downwash on the retreating side, therefore a negative longitudinal cyclic control angle is needed to eliminate the resulting aerodynamic rolling moment. See Fig. 3 (b) for the vortex orientation, and also for $\psi_V = \pi$, which represents a change of sense of rotation as experienced by the rotor. Therefore, as shown in Fig. 5 (b), the required longitudinal cyclic control angle changed its sign as well.

Keeping $\psi_V = 0$ and shifting the vortex to $y_{V0} = 1$, then the entire rotor disk is immersed in its downwash with the maximum on the advancing side, thus generating a large lateral asymmetry with more loss of lift on the advancing than on the retreating side and the associated aerodynamic rolling moment must be compensated by a positive longitudinal cyclic control angle, as shown in the graph. Contrary, shifting the vortex to the opposite end of the disk to $y_{V0} = -1$ the entire disk is immersed in its upwash with the maximum on the retreating side.

This generates a large lateral asymmetry with more increase of lift on the retreating than on the advancing side and the associated aerodynamic rolling moment again must be compensated by a positive longitudinal cyclic control angle, as shown in the graph. Further outside positions diminish the vortex-induced velocities, therefore the impact on the aerodynamic rolling moment, and as well the amount of longitudinal cyclic control angle required to mitigate this and the curves asymptotically approach zero for very large distances of the vortex as required. Vortex orientation angles with $\psi_V = \pm 0.5\pi$ do not generate aerodynamic rolling moments and therefore both curves of the longitudinal cyclic control angle are zero.

Like the longitudinal cyclic control angle, the lateral cyclic control angle in hover significantly depends on both the vortex distance to the rotor center and its orientation relative to the rotor x-axis. Now only longitudinal asymmetries of vortex-induced velocities generate aerodynamic pitching moments. Therefore, vortex orientation parallel to the rotor x-axis, i.e. $\psi_V = 0, \pi$, generate longitudinal symmetry of vortex-induced velocities, therefore no aerodynamic pitching moment and thus zero lateral cyclic control is needed. Four cuts at vortex orientation angles $\psi_V = 0, \pm 0.5\pi, \pi$ are shown in Fig. 6 (b) together with a vortex and its swirl velocity field placed in the rotor center.

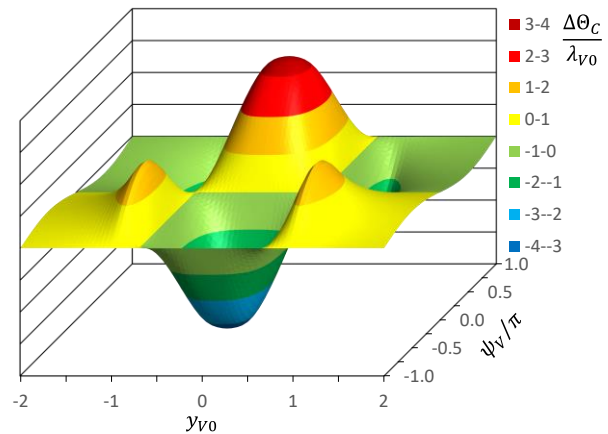(a) Range of vortex position and orientation angles

(b) Selected vortex orientation angles

Fig. 5. Longitudinal cyclic control angle for vortex disturbance rejection on rotor aerodynamic rolling moment.

(a) Range of vortex position and orientation angles
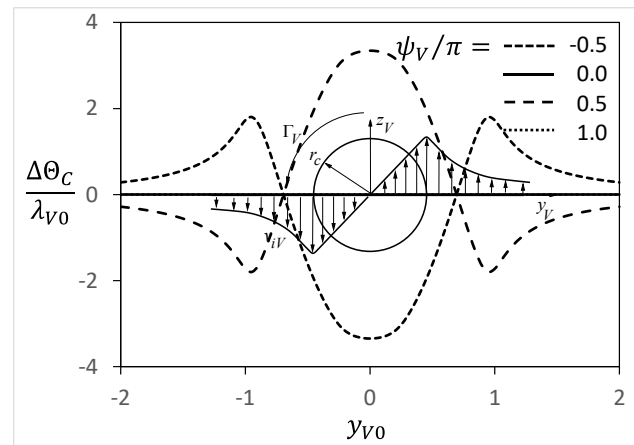

(b) Selected vortex orientation angles

Fig. 6. Lateral cyclic control angle for vortex disturbance rejection on rotor aerodynamic pitching moment.

Finally, the lateral cyclic control angle required for vortex disturbance rejection on the aerodynamic rotor pitching moment, related to the vortex strength $\Delta\Theta_C / \lambda_{V0}$, is shown in Fig. 6 (a) for the same range of y_{V0} and ψ_V as before.

For $\psi_V = -0.5\pi$ this generates a large upwash on the rear side of the rotor and as much downwash on the front side, therefore a negative lateral cyclic control angle is needed to eliminate the resulting aerodynamic pitching moment. See Fig. 3 (b) for the vortex orientation, and also for $\psi_V = +0.5\pi$, which represents a change of sense of rotation as experi-

enced by the rotor. Therefore, as shown in Fig. 6 (b), the required lateral cyclic control angle changed its sign as well. Vortex orientation angles with $\psi_V = 0, \pm\pi$ do not generate aerodynamic pitching moments and therefore both curves of the lateral cyclic control angle are zero.

3.2. Parameter variations in hover

The essential parameters to be investigated are the vortex core radius and the begin and end of the airfoiled portion of the rotor blade. Especially in hover the vortex orientation angle is unimportant, therefore it is set to $\psi_V = 0$ throughout this section.

First, the influence of the effective begin A and the effective end B of the rotor blade on the collective control angle $\Delta\Theta_0/\lambda_{V0}$ will be examined and results are shown in Fig. 7 (a), to be compared with Fig. 4 (b). Black lines vary the effective begin of the blade from the rotor hub at $A = 0$ to 0.6 while the effective end remains at the blade tip at $B = 1$.
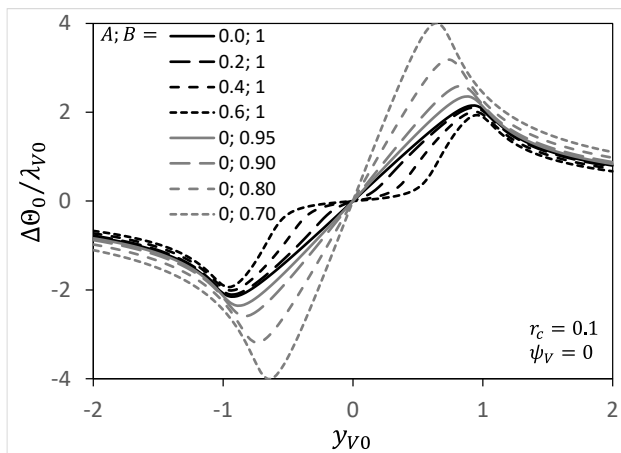
(a) Variation of begin A and end B of the rotor blade
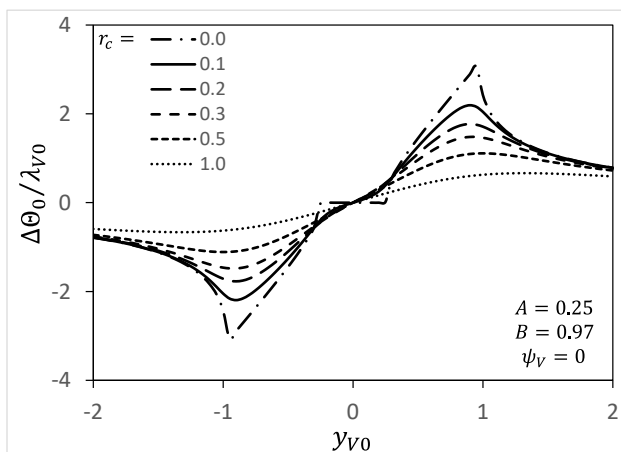
(b) Variation of the core radius r_c

Fig. 7. Collective control angle for vortex disturbance rejection on rotor thrust.

This blade root cutout variation is most visible for vortex positions within this cutout region, where inside of it no vortex-induced lift is generated anymore and therefore with increasing A the curves become progressively flatter in this region. For vortex positions towards either side of the rotor disk and outside of them the results are very close together, because the major vortex impact is at the outer portion of the blade that remains unmodified.

The grey lines in Fig. 7 (b) keep the effective begin at the hub $A = 0$ and vary the effective end of the blade from $B = 0.95$ down to 0.7, which is equivalent to a reduced blade length at constant rotational speed. The maximum impact of the vortex remains at positions close to the effective blade tip, and it may be surprising at first glance that the magnitude of control required to mitigate the vortex impact on rotor thrust is growing. However, considering that the largest vortex-induced inflow angles occur inboard (recall that $\phi \approx \lambda_{iV}/r$) and the smallest outboard, the average vortex-induced inflow angle will grow when clipping off the blade end, which in reverse requires a larger blade pitch angle to compensate it.

Keeping the blade constant with $A = 0.25$ and $B = 0.97$ which is closest to practical applications and which was used in Fig. 4 (b) before, the core radius is varied next from a value very close to zero $r_c \approx 0$ (which is out of the scope of application due to violation of the small angle assumption, but shown here for completeness) up to the radius of the entire blade $r_c = 1$ and results are shown in Fig. 7 (b). Zero core radius represents a potential vortex with induced velocities approaching infinity when the core radius nears zero, see Eq. (1). This of course generates the largest amount of vortex-induced inflow angle even at the blade tips, thus the largest, yet finite amount of collective control is needed to retrim the rotor. Interesting: vortex positions inside the root cutout lead to almost constant collective control angles around zero in this regime, in agreement with Fig. 7 (a).

With increasing the core radius, the peak vortex-induced velocities become progressively smaller, with it the vortex-induced impact on section lift and the overall impact on thrust is accordingly reducing. Therefore, less and less collective control angle is required to mitigate the vortex impact on trim with increasing core radius.

The same variations are shown next at the example of the longitudinal cyclic control angle $\Delta\Theta_S/\lambda_{V0}$ only, as it is the same impact on the lateral cyclic control angle for vortex orientation angle $\psi_V = -0.5\pi$ instead of $\psi_V = 0$ used here, see Fig. 5 (b) and Fig. 6 (b). $\Delta\Theta_S$ is needed to counteract the vortex-

induced aerodynamic rolling moment while $\Delta\Theta_C$ is needed to eliminate the respective aerodynamic pitching moment. First, the impact of the blade root cutout is shown in Fig. 8 (a) by the black lines again. As in the collective control angle, the inner portion of the curve flattens out with increasing root cutout A for the same reasons explained before in accordance with Fig. 7 (a).
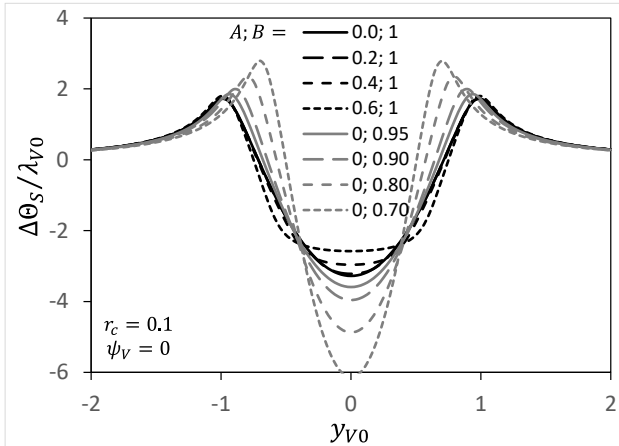
(a) Variation of begin A and end B of the rotor blade
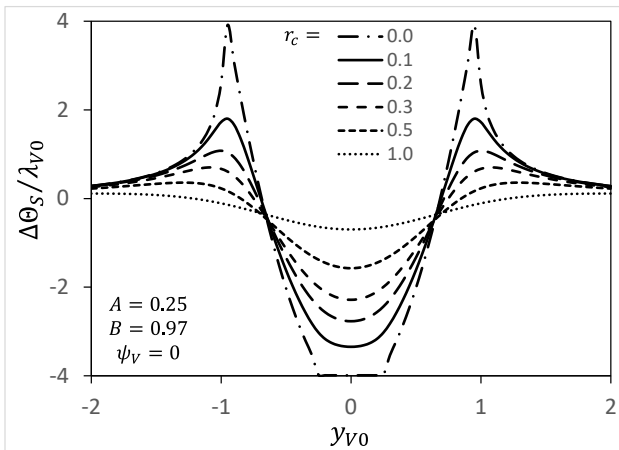
(b) Variation of the core radius r_c

Fig. 8. Longitudinal cyclic control angle for vortex disturbance rejection on rotor thrust.

The variation of the effective end of the blade B is again represented by the grey lines and like the growth of the collective control angle in Fig. 7 (a) the longitudinal cyclic control angle required to mitigate the vortex-induced aerodynamic rolling moment is growing with blade length reduction. Again, the effects are due to the same physical reasons explained before.

It is important to know that the cyclic control angles (longitudinal and lateral) correspond to the vortex-induced inflow gradients (lateral and longitudinal, respectively) across the rotor disk, while the collective control angle is related to the mean value of the vor-

tex-induced inflow within the rotor disk.

Finally, the vortex core radius is varied and results shown in Fig. 8 (b). As was the case in Fig. 7 (b) for the collective control angle, zero core radius generates the largest inflow gradients because near the core radius the induced velocities approach infinity, however, confined to an as well infinite small area of the disk. With growing core radius, the peak vortex-induced velocities become smaller, thus the inflow gradient as well and accordingly less amount of longitudinal cyclic control is needed to retrim the rotor.

3.3. Forward flight

The same investigations as in the two preceding sections for hover are now performed for the forward flight case with an advance ratio of $\mu = 0.3$, representative for a cruise condition of helicopters.

The major differences with respect to the hovering case stem from the significantly larger tangential velocities and thus dynamic pressure on the advancing side of the rotor and simultaneously significantly less on the retreating side.

The vortex-induced section lift is proportional to the dynamic pressure times the inflow angle, $V_T^2\phi \approx V_T v_{iV}$, that will be balanced during retrim by the lift generated by the control angles, which is proportional to $V_T^2\Theta$. These simple proportionalities help in understanding the results due to the lateral asymmetry of dynamic pressure in forward flight. In non-dimensional form this is expressed by

$$
\begin{aligned}
L'(\lambda_{iV}) &\sim (r + \mu\sin\psi)\lambda_{iV}(r,\psi) \\
L'(\Delta\Theta) &\sim (r + \mu\sin\psi)^2\Delta\Theta(\psi)
\end{aligned}
$$
(11)

Note that the treatment in the reversed flow area on the retreating side of the rotor is erroneous from a physical point of view, but comes along with very low dynamic pressures compared to the rest of the disk and therefore the overall error is negligible for all advance ratios of conventional helicopters as outlined in classical textbooks; also, the affected region is further reduced by the blade root cutout.

As in section 3.1 the following parameters are kept constant throughout section 3.3 and in the range of figures from Fig. 9 to Fig. 11: $A = 0.25, B = 0.97, r_c = 0.1$; their variation is addressed in section 3.4.

Like in Fig. 4 (a) for the hovering rotor, the collective control angle for vortex disturbance rejection on rotor thrust, related to the vortex strength $\Delta\Theta_0/\lambda_{V0}$, is shown in Fig. 9 (a) for the entire range of the aforementioned vortex position relative to the rotor center

y_{V0} and the range of vortex orientation angle ψ_V once around the rotor, now for an advance ratio of $\mu = 0.3$. The essential behavior is quite similar to that of hover in Fig. 4 (a), but the asymmetry of dynamic pressure caused some variations that can better be seen and understood in the four cuts at vortex orientation angles $\psi_V = 0, \pm 0.5\pi, \pi$ that are shown in Fig. 9 (b).
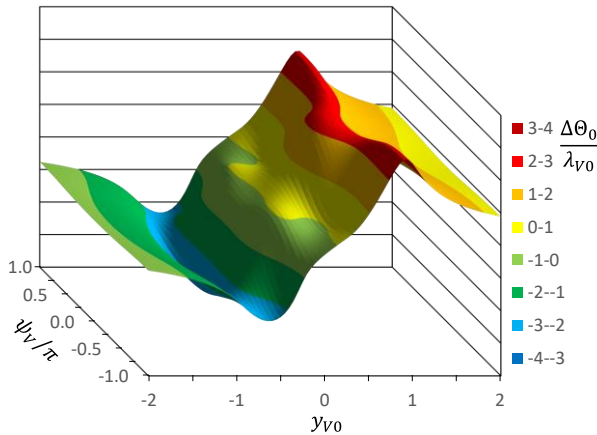
(a) Range of vortex position and orientation angles
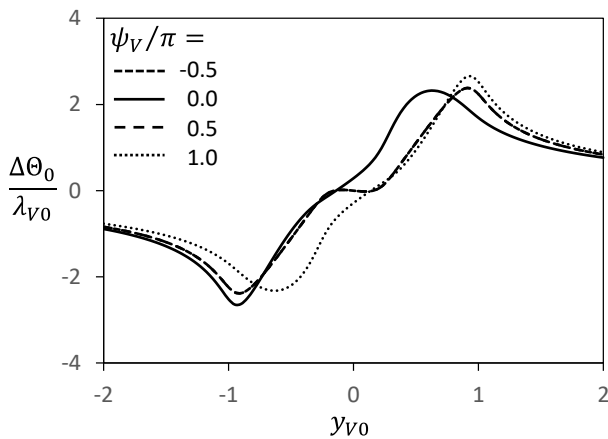
(b) Selected vortex orientation angles

Fig. 9. Collective control angle for vortex disturbance rejection on rotor thrust.

When the vortex is oriented parallel to the rotor y-axis, i.e. $\psi_V = \pm 0.5\pi$ (see Fig. 3 (b)), the largest difference to Fig. 6 (b) is found for vortex positions in the region of the root cutout. This is the area where the largest differences in dynamic pressure exist between advancing and retreating side. Vortex positions at the front or back side of the rotor have the largest vortex-induced velocities close to the x-axis of the rotor, where the differences of dynamic pressure are very small.

A vortex orientation parallel to the x-axis of the rotor, i.e. $\psi_V = 0, \pi$ (see Fig. 3 (b)) flattens out the peak for vortex positions on the advancing side and shifts it

more inboard, while the peak itself is little larger than in hover, compare to Fig. 4 (b). A vortex position on the retreating side increases the peak relative to hover more significantly, while keeping its position.

Both phenomena can partly be explained with the difference in lift generation outlined in Eq. (11). The lift change caused by the vortex on the advancing side increases linearly with the advance ratio, while a lift change due to the control angle increases proportional to the square of it. Therefore, less control angle is needed to mitigate the lift caused by the vortex.

Contrary on the retreating side: the lift caused by the vortex is linearly reducing with the advance ratio, but the lift due to the control angle is reducing proportional to the square of it. This loss of effectiveness requires more control angle for compensation of the vortex-induced lift. Another contribution in the collective control angle stems from the coupling of longitudinal cyclic control and collective control in forward flight by the coefficients a_{12}, a_{21} in Eq. (7). Any change of thrust caused by the collective control angle in forward flight also introduces an aerodynamic rolling moment that requires a longitudinal cyclic control angle to eliminate it and vice versa; and the higher the advance ratio, the stronger this effect.

Like in Fig. 5 (a) for the hovering rotor, the longitudinal cyclic control angle for vortex disturbance rejection on rotor aerodynamic rolling moments, related to the vortex strength $\Delta\Theta_S/\lambda_{V0}$, is shown in Fig. 10 (a). It can be observed that the difference in dynamic pressure generates some asymmetry throughout the entire range of vortex positions that is largest when the vortex is parallel to the rotor x-axis, i.e. for $\psi_V = 0, \pi$ (see Fig. 3 (b)).

Four cuts across Fig. 10 (a) at vortex orientation angles $\psi_V = 0, \pm 0.5\pi, \pi$ are shown in Fig. 10 (b), to be compared with the hovering case shown in Fig. 5 (b). The longitudinal cyclic control angle is most sensitive to lateral asymmetry of dynamic pressure because of $\Theta_S \sin\psi$ and it is largest where the dynamic pressure is largest, i.e. at $\psi = \pm 0.5\pi$ where $\sin\psi = \pm 1$. For the same reasons as explained before the peak value of longitudinal cyclic control for vortex positions near the blade tip on the advancing side is less than in hover and larger than in hover for vortex positions near the blade tip on the retreating side. The overall maximum values were obtained in hover around $y_{V0} = 0$. In forward flight these largest values are shifted to vortex positions little more on the advancing side of the rotor, also, they are larger than in hover due to the coupling with the collective control angle.
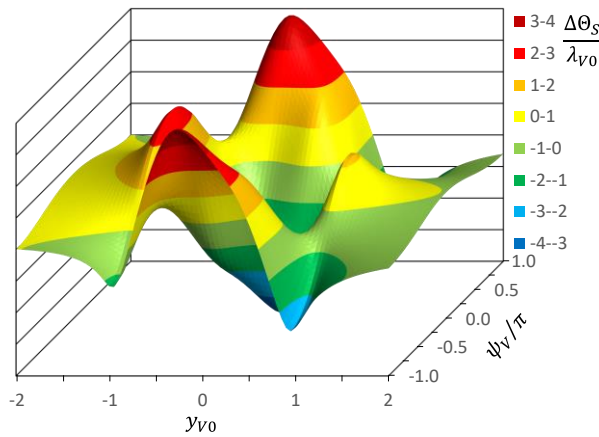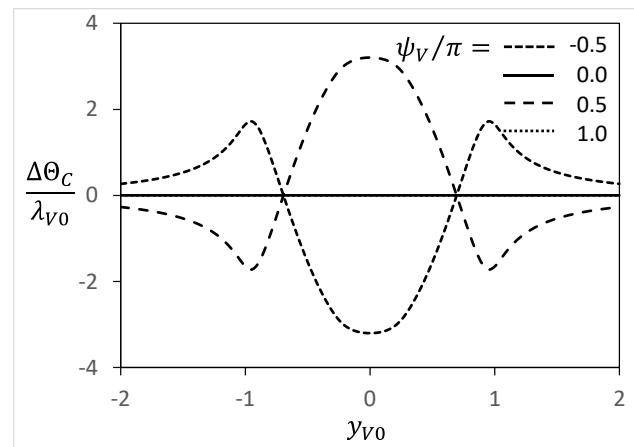
(a) Range of vortex position and orientation angles
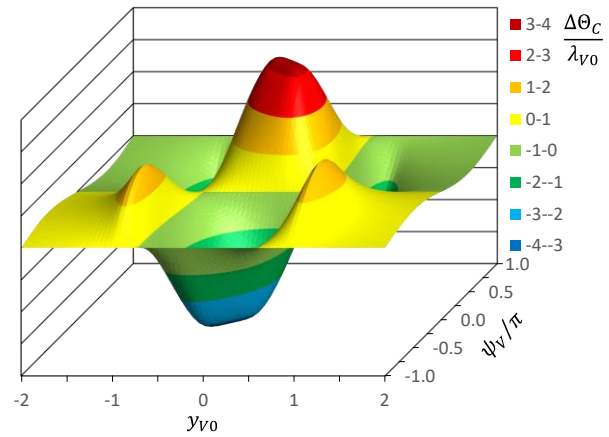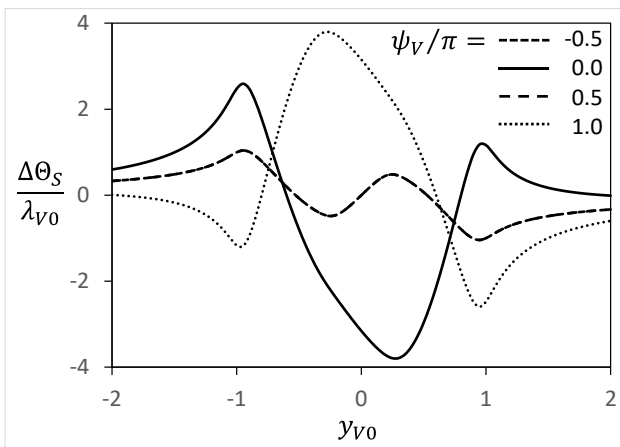
(b) Selected vortex orientation angles

Fig. 10. Longitudinal cyclic control angle for vortex disturbance rejection on rotor aerodynamic rolling moment.

(a) Range of vortex position and orientation angles

(b) Selected vortex orientation angles

Fig. 11. Lateral cyclic control angle for vortex disturbance rejection on rotor aerodynamic pitching moment.

It is interesting to note that the longitudinal cyclic control angle is also required to retrim for vortex orientation angles parallel to the rotor y-axis, i.e. $\psi_V = \pm 0.5\pi$. Recall from Eq. (7) that the collective control and the longitudinal cyclic control angles are mutually coupled in forward flight and therefore any thrust change caused by collective control also introduces an aerodynamic rolling moment. This needs a longitudinal cyclic control angle for compensation, which in return generates a change in thrust that requires some collective control to eliminate it.

Finally, the lateral cyclic control angle required to retrim the rotor in forward flight due to the vortex influence $\Delta\Theta_C/\lambda_{V0}$ is shown in Fig. 11 (a), to be compared with its equivalent in hover shown in Fig. 6 (a).

It is obvious that the forward flight and its associated asymmetry of dynamic pressure has much less impact on the lateral cyclic control angle than on the collective or longitudinal cyclic control angles shown in Fig. 9 (a) and Fig. 10 (a).

This is easily explained by the physics behind, since the lateral cyclic control angle $\Theta_C \cos\psi$ is largest in the front and rear of the disk where the dynamic pressure exhibits only small differences between the advancing and the retreating side, and $\cos\psi = 0$ where the largest asymmetry exists in dynamic pressure, i.e. at $\psi = \pm 0.5\pi$.

Four cuts across Fig. 11 (a) at vortex orientation angles $\psi_V = 0, \pm 0.5\pi, \pi$ are shown in Fig. 11 (b), to be compared with the hovering case shown in Fig. 6 (b). At first glance they look alike, but actually the peak values for vortex positions in the rotor center are little less in forward flight than in hover. The same is true for the peak values occurring for vortex positions near the blade tip of the front or rear of the rotor disk.

However, the lateral cyclic control angle is independent of the collective and longitudinal cyclic control angles as seen from Eq. (7). Also, for any vortex positions with a vortex orientation parallel to the x-

axis, i.e. for $\psi_V = 0, \pi$, there is no impact of the advance ratio seen and the lateral cyclic control angle remains zero for all vortex positions with this orientation, as is the case in hover. From Eq. (7): $\Delta\Theta_C/\lambda_{V0} \sim 1/(-a_{33})$, Eq. (8) and with the values for A, B inserted, we obtain: $-a_{33} = 0.11 + 0.055\mu^2$. For the advance ratio investigated here: $\mu = 0.3$; $\mu^2 = 0.09$. Therefore, in hover $-a_{33} = 0.11$ and in this forward flight case $-a_{33} = 0.115$, a little larger, and therefore $\Delta\Theta_C$ is little less than in hover, but the influence is rather small.

3.4. Parameter variations in forward flight

The essential parameters to be investigated are the vortex core radius and the begin and end of the air-foiled portion of the rotor blade. The fundamental impact of the vortex orientation angle was outlined in the sections before, therefore it is set to $\psi_V = 0$ only throughout this section.

First, the variation of the effective begin A and the effective end B of the rotor blade will be examined with respect to the collective control angle $\Delta\Theta_0/\lambda_{V0}$ and results are shown in Fig. 12 (a), to be compared with the equivalent in hover of Fig. 7 (a). Black lines vary the effective begin of the blade from the rotor hub at $A = 0$ to 0.6 while the effective end remains at the blade tip at $B = 1$, and the core radius is kept constant at $r_c = 0.1$.

The fundamental effect of increasing the root cutout is quite similar to the hovering case, combined with the observations due to the advance ratio already made with Fig. 9 (b). Vortex positions at the blade tip of the retreating side require larger collective control than in hover, because the control effectiveness there is less than in hover ($L' \sim (r - \mu)^2 \Theta$), while vortex positions at the blade tip on the advancing side require less collective control angle, because there the control effectiveness is larger than in hover ($L' \sim (r + \mu)^2 \Theta$).

Keeping the begin of the blade at the hub center and varying the effective end of the blade is represented by the grey lines in Fig. 12 (a). The hump in the range $-0.3 < y_{V0} < 0$ in all curves with $A = 0$ is caused by the erroneous treatment of the reversed flow region as mentioned in section 3.3 following Eq. (11) and may thus be ignored; for root cutouts of $A \geq 0.2$ this vanishes. The observations for reducing the effective length of the blade in forward flight are essentially the same as in hover: the maximum values of collective control angles needed to retrim the rotor are moving inboard together with the reduction of blade length and the magnitude is increasing for the same reasons explained in conjunction with Fig. 7 (a) in hover.

Finally, the effect of variation of the core radius r_c is shown in Fig. 12 (b), to be compared with the equivalent in hover of Fig. 7 (b). For the same reasons as in hover the peak values are diminishing with increasing vortex core radius, which is modified by effects due to the asymmetry in dynamic pressure. Therefore, vortex positions on the retreating side cause larger collective control angles than in hover, and positions on the advancing side require smaller ones than in hover.
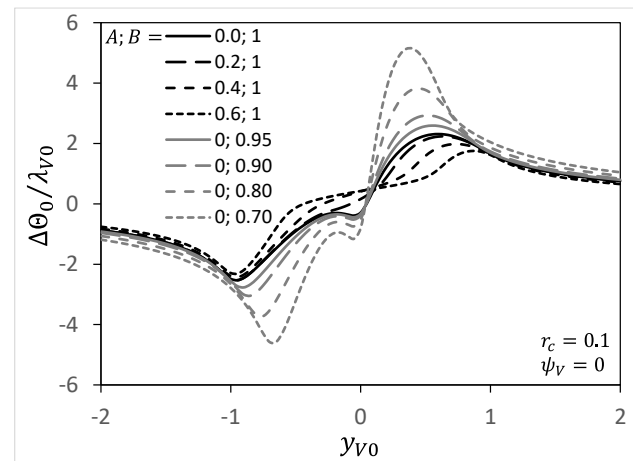
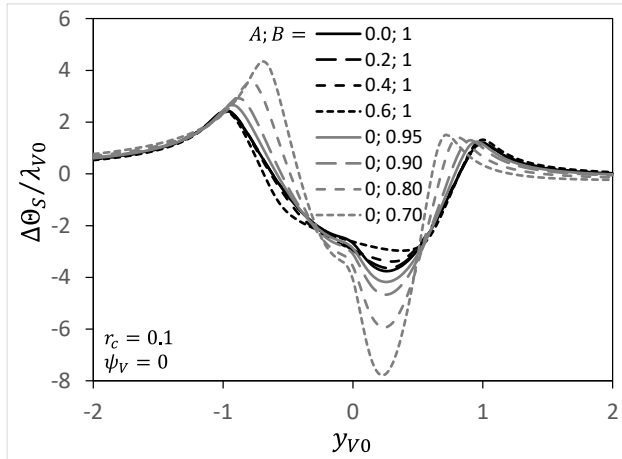(a) Variation of begin A and end B of the rotor blade
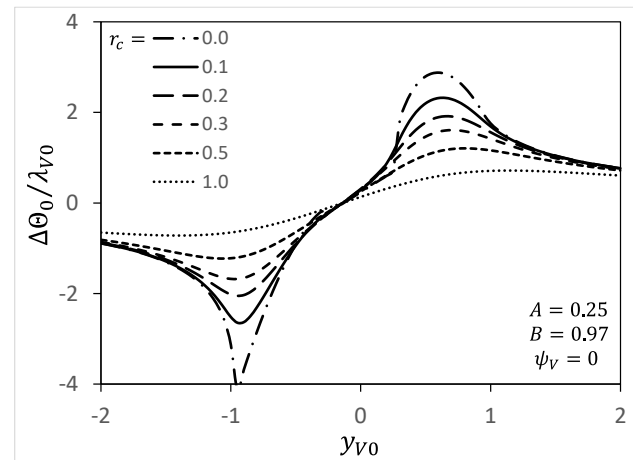
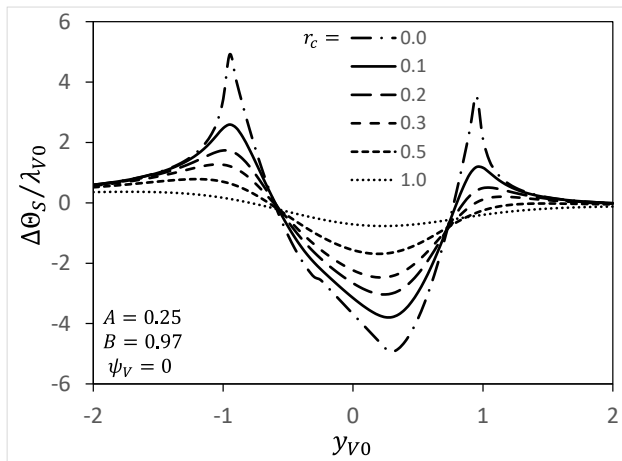(b) Variation of the core radius r_c

Fig. 12. Collective control angle for vortex disturbance rejection on rotor thrust.

The same variations of parameters are shown in Fig. 13 for the longitudinal cyclic control angle required to retrim the rotor $\Delta\Theta_S/\lambda_{V0}$, to be compared with the equivalent in hover given before in Fig. 8. Again, the fundamental variations are quite similar to the hovering case, but modified by the effect due to the asymmetry of dynamic pressure in a similar manner as found in the collective control angle just before. Therefore, longitudinal cyclic control angles for vortex positions on the retreating side are larger than for vortex positions on the advancing side.

The peak values move inboard with shrinking blade length, while the effect of varying the root cutout is much less visible than in the collective control angle. This is because here the aerodynamic moment with respect to the hub center is of interest, i.e. rL', and since $r \to 0$ towards the hub center the inner regions are much less important than the blade tip area where $r \to 1$.

(a) Variation of begin A and end B of the rotor blade


(b) Variation of the core radius r_c

Fig. 13. Longitudinal cyclic control angle for vortex disturbance rejection on rotor thrust.

The last variation is a sweep of advance ratios while keeping all other parameters constant: $A = 0.25$, $B = 0.97$, $r_c = 0.1$, $\psi_V = 0$. This is shown in Fig. 14 (a) for the collective control angle $\Delta\Theta_0/\lambda_{V0}$ and in Fig. 14 (b) for the longitudinal cyclic control angle $\Delta\Theta_S/\lambda_{V0}$. The results for the hovering case $\mu = 0$ were already shown in Fig. 7 (b) and in Fig. 8 (b), and the results for $\mu = 0.3$ were already shown in Fig. 12 (b) and in Fig. 13 (b).
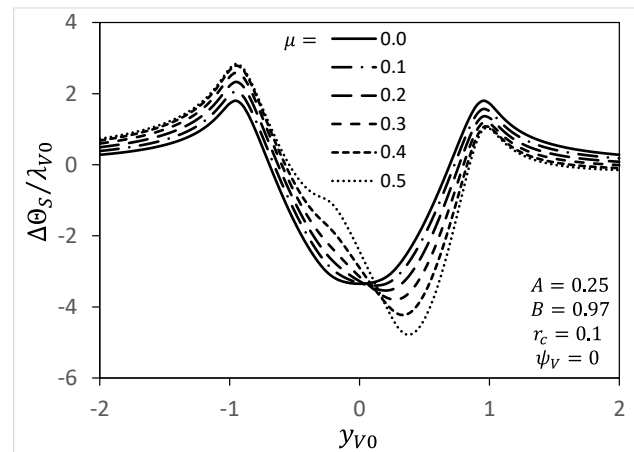
With increasing advance ratio the curves are progressively modified, the reason lies in the dynamic pressure which is proportional to:

$$(r + \mu \sin\psi)^2 = r^2 + 2r\mu\sin\psi$$
$$(12) \qquad + \frac{\mu^2}{2}(1 - \cos 2\psi)$$

This is proportional to both μ and to μ^2, which explains the progressive modification with increasing μ. The hump in the range $0 > y_{V0} > -\mu$ in the curves for $\mu = 0.4$ and 0.5 is due to the erroneous treatment of the reversed flow region and may be ignored. The former observations of smaller control magnitude for vortex positions on the advancing side and larger magnitude for positions on the retreating side is well seen in the longitudinal cyclic control angle.
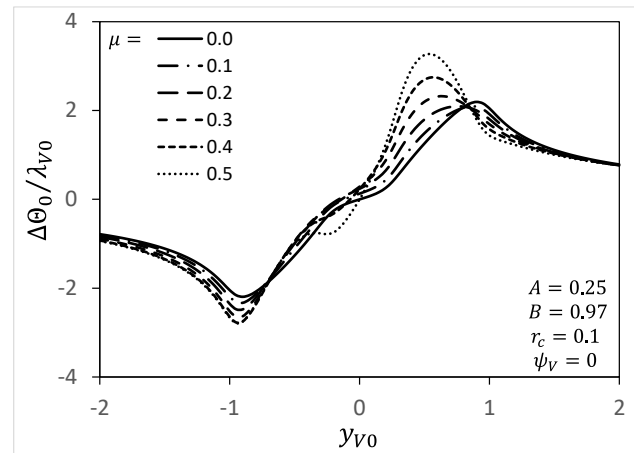
(a) Collective control angle

(b) Longitudinal cyclic control angle

Fig. 14. Rotor control angles for vortex disturbance rejection on rotor trim, variation of the advance ratio.

However, with increasing advance ratio the collective control angle and the longitudinal cyclic control angle are more and more coupled by the system matrix elements a_{12} and a_{21} in Eqs. (7) and (8), causing the increase of the peak values in the collective control angle for vortex positions on both the advancing and the retreating side.

3.5. Some practical examples

Assume a tanker aircraft of the size of an Airbus A400M with a mass of $m = 130$ tons, a wing span of $b = 42$ m, and a flight speed of $V_\infty = 80$ m/s. Then the vortex circulation in flight at sea level can be estimated to $\Gamma_V = mg/(\rho b V_\infty) \approx 300$ m²/s and the core radius may be assumed as 0.5 m near to the aircraft and 2 m at a farer distance away from it.

A helicopter of the size Bo105 with $R = 5$ m radius and a tip speed of $\Omega R = 220$ m/s following the aircraft at the same speed will have the following parameters, see Eq. (5): $\lambda_{V0} = 0.0434$; $r_c = 0.1$; $\mu = 0.36$; $A = 0.25$; $B = 0.97$. The maximum values of control angles become $\Delta\Theta_0 \approx -2.7\lambda_{V0} \approx -6.7$ deg and $\Delta\Theta_S \approx -4\lambda_{V0} \approx -10$ deg, Values for $\Delta\Theta/\lambda_{V0}$ are taken from Fig. 12 to Fig. 14. The larger core radius farer away from the aircraft leads to $r_c = 0.4$; $\Delta\Theta_0 \approx -1.5\lambda_{V0} \approx -3.7$ deg and $\Delta\Theta_S \approx -2.1\lambda_{V0} \approx -5.2$ deg.

A much larger helicopter of size CH-53 with radius $R = 11$ m and the same blade tip speed $\Omega R = 220$ m/s will have for the small core radius near the aircraft: $\lambda_{V0} = 0.0197$; $r_c = 0.045$; $\Delta\Theta_0 \approx -3.3\lambda_{V0} \approx -3.7$ deg and $\Delta\Theta_S \approx -4.5\lambda_{V0} \approx -5.1$ deg and for the large core radius farer away from the aircraft $r_c = 0.18$; $\Delta\Theta_0 \approx -2.2\lambda_{V0} \approx -2.5$ deg and $\Delta\Theta_S \approx -3.3\lambda_{V0} \approx -3.7$ deg.

Because in fast forward flight the control margin until the hard stops of the control system are not very large these additional control angles may exceed the control capability of the pilot in case of an unfortunate vortex sense of rotation.

However, these are the extreme values representing the theoretical worst case. In practice, especially at lower advance ratios, mutual interaction between the vortex and the rotor wake alleviate the vortex influence to some degree, less at high advance ratios, but increasingly more at small advance ratios, as was recently demonstrated in [18]. Also, the control margins until the hard stops are reached are larger in flight with small to moderate advance ratios.

4. CONCLUSIONS

In this paper the impact of a vortex interacting with a rotor is investigated, based on an entirely analytic solution of the vortex-rotor interaction problem. The major findings are listed below.

- An analytic solution for the in-plane vortex-rotor interaction problem is given for arbitrary vortex orientation with respect to the rotor longitudinal direction and arbitrary position relative to the rotor hub.

- Based on this, the collective, longitudinal and lateral cyclic control angles required to retrim the rotor during a vortex-rotor interaction can be computed.

- These control angles are linear proportional to the non-dimensional vortex strength λ_{V0}, which relates the vortex circulation Γ_V to rotor operational parameters blade tip speed times the radius: ΩR^2.

- Therefore, the larger λ_{V0}, the larger the control angles required to retrim the rotor.

- Another important parameter is the non-dimensional vortex core radius r_c, which relates the physical vortex core radius to the radius of the interacting rotor.

- The smaller r_c, the larger become the vortex-induced airloads on the rotor blades and the larger become the control angles required to retrim the rotor.

- Therefore, for a given vortex and constant blade tip speed: the smaller the helicopter, the larger the control angles required to retrim the rotor.

- Also, for a given vortex and a constant rotor radius: the smaller the blade tip speed, the larger the control angles required to retrim the rotor.

5. REFERENCES

AHS = American Helicopter Society
ERF = European Rotorcraft Forum

[1] Dunham, R.E., Holbrook, G.T., Mantay, W.R., Campbell, R.L., Van Gunst, R.W.: Flight-Test Experience of a Helicopter Encountering an Airplane Trailing Vortex. 32nd Annual National V/STOL Forum of the AHS., Washington, DC (1976)

[2] Mantay, W.R., Holbrook, G.T., Campbell, R.L., Tamaine, R.L.: Helicopter Response of an Airplane's Trailing Vortex. J. Aircraft, 14(4), 357-363 (1977)

[3] Saito, S., Azuma, A., Kawachi, K., Okuno, Y.: Study of the Dynamic Response of Helicopters to a Large Airplane Wake. 12th ERF, Garmisch-Partenkirchen, Germany (1986)

[4] Azuma, A., Saito, S., Kawachi, K.: Response of a Helicopter to the Tip Vortices of a Large Airplane. VERTICA, 11(1), 65-76 (1987)

[5] Saito, S., Azuma, A., Okuno, Y., Hasegawa, T.: Numerical Simulations of Dynamic Response of Fixed and Rotary Wing Aircraft to a Large Airplane Wake. 13th ERF, Arles, France (1987)

[6] Turner, G.P., Padfield, G.D., Harris, M.: Encounters with Aircraft Vortex Wakes; The Impact on Helicopter Handling Qualities. J. Aircraft, 39(5), 839–849 (2002)

[7] Padfield, G.D., Manimala, B., Turner, G.P.: A Severity Analysis for Rotorcraft Encounters with Vortex Wakes. J. AHS, 49(4), 445–456 (2004)

[8] Lawrence, B., Padfield, G.D.: Wake Vortex Encounter Severity for Rotorcraft in Approach and Landing. 31st ERF, Florence, Italy (2005)

[9] Whitehouse, G.R., Brown, R.E.: Modelling a Helicopter Rotor's Response to Wake Encounters. The Aeronautical J., 108(1079), 15-26 (2004)

[10] Bakker, R., Visingardi, A., van der Wall, B.G., Voutsinas, S., Basset, P. M., Campagnolo, F., Pavel, M., Barakos, G., White, M.: Wind Turbine Wakes and Helicopter Operations - An Overview of the Garteur HC-AG23 Activities. 44th ERF, Delft, Netherlands (2018)

[11] van der Wall, B.G., van der Wall, L.B.: Analytical Estimate of Rotor Controls Required for a Straight Vortex Disturbance Rejection. J. AHS, 62(1), 015001 (2017)

[12] van der Wall, B.G.: Analytical Estimate of Rotor Blade Flapping Caused by a Straight Vortex Disturbance. J. AHS, 62(4), 045001 (2017)

[13] van der Wall, B.G., van der Wall, L.B.: Analytic Solution of In-Plane Vortex-Rotor Interactions with Arbitrary Orientation and its Impact on Rotor Trim. CEAS Aeronaut. J., online first, (2021)

[14] van der Wall, B.G., Lehmann, P.: About the Impact of Wind Turbine Blade Tip Vortices on Helicopter Rotor Trim and Rotor Blade Motion. CEAS Aeronaut. J., 9(1), 67-84 (2018)

[15] van der Wall, B.G.: Wind Turbine Wake Vortex Influence on Safety of Small Rotorcraft. The Aeronautical J., 123(1267), 1374-1395 (2019)

[16] van der Wall, B.G.: Rotor Thrust and Power Variations During In-Plane and Orthogonal Vortex Interaction. 7th Asian/Australian Rotorcraft Forum, Jeju Island, South Korea (2018)

[17] Vatistas, G.H., Kozel, V., Mih, W.C.: A Simpler Model for Concentrated Vortices. Experiments in Fluids, 11(1), 73-76 (1991)

[18] van der Wall, B.G.: Impact of Vortex - Wake Interference on Rotor Trim, VFS Transformative Vertical Flight 2020 - Aeromechanics for Advanced Vertical Flight Technical Meeting, San Jose, CA (2020)

Biographies

Berend G. van der Wall is Senior Scientist at the German Aerospace Center (DLR), where he started his career in 1986. His education includes a Master's degree from the University of Maryland in 1991 and he obtained his Diploma in 1986 and Ph.D. degree from TU Braunschweig in 1999. His subjects of work combine the development of DLR's S4 rotor simulation code with about 25 experiments of large-scale rotor and helicopter models in the Large Low-Speed Facility of the German-Dutch Wind Tunnel, mostly within international cooperation. He headed the US/German and Korean/German MoU's on Rotorcraft Aeromechanics from 2006-2012, and the DLR/Onera Research Field 5 "The Innovative Rotorcraft" since 2002.

Berend earned major credits in higher harmonic rotor control technology with the well-known HART II test and its International Workshop, honored by the AHS Howard Hughes and AgustaWestland International Fellowship Awards in 2004 and 2012. Since 2000 he is interested in rotorcraft history and received the AHS Bernard Lindenbaum Best Historical Paper Award in 2016 and 2020. The German Aerospace Society honored him 2019 with the Honorary Pin of the German Aviation.

His achievements include the patented design of a low noise rotor blade ERATO that finally became the Blue Edge Rotor blade on Airbus Helicopters brand new H160, a patent on the multi-swashplate control technology called META, a patent on advanced prescribed wake formulation, and some others.

Since 2007 he is lecturer at the TU Braunschweig for "Helicopter Aerodynamics" and "Rotor Dynamics" and became honorary professor there in 2014. He authored two textbooks on helicopter aerodynamics and rotor dynamics and is editor of a book about German Rotating-Wing Developments during WW II.

Lennert B. van der Wall studied electrical engineering at TU Braunschweig, obtained his Bachelor degree in 2017 and has almost finished the Masters program. His skills in mathematics helped to provide closed-form analytical solutions to so far unsolved problems and made him co-author of two Journal articles and two conference papers.